Research Article | Vol. 26, No. 9 | 30 Apr 2018 | OPTICS EXPRESS 12092
Optics EXPRESS

Iterative matrix algorithm for high precision temperature and force decoupling in multi-parameter FBG sensing

BARBARA HOPF,[1,*] FRANZ J. DUTZ,[1] THOMAS BOSSELMANN,[2] MICHAEL WILLSCH,[2] ALEXANDER W. KOCH,[3] AND JOHANNES ROTHS[1]

[1]*Munich University of Applied Sciences, Photonics Laboratory, D-80335 Munich, Germany*
[2]*Siemens AG, Corporate Technology, CT RDA SII SSI-DE, D-91058 Erlangen, Germany*
[3]*Technical University of Munich, Institute for Measurement Systems and Sensor Technology, D-80290 Munich, Germany*
[*]*barbara.hopf@hm.edu*

Abstract: A new iterative matrix algorithm has been applied to improve the precision of temperature and force decoupling in multi-parameter FBG sensing. For the first time, this evaluation technique allows the integration of nonlinearities in the sensor's temperature characteristic and the temperature dependence of the sensor's force sensitivity. Applied to a sensor cable consisting of two FBGs in fibers with 80 µm and 125 µm cladding diameter installed in a 7 m-long coiled PEEK capillary, this technique significantly reduced the uncertainties in friction-compensated temperature measurements. In the presence of high friction-induced forces of up to 1.6 N the uncertainties in temperature evaluation were reduced from several degrees Celsius if using a standard linear matrix approach to less than 0.5°C if using the iterative matrix approach in an extended temperature range between −35°C and 125°C.

OCIS codes: (060.2370) Fiber optics sensors, (060.3735) Fiber Bragg gratings.

References and links

1. R. Kashyap, *Fiber Bragg gratings*, 2nd ed. (Academic, 2010).
2. X. Qiao, Z. Shao, W. Bao, and Q. Rong, "Fiber Bragg grating sensors for the oil industry," Sensors (Basel) **17**(3), 429 (2017).
3. G.-H. Lv, S.-H. Shang, X. Jiang, O. Jin-Ping, C. Yang, C. D. Li, and W. Xu, "FBG temperature and pressure sensing system for hot water pipeline of petrochemical factory," in Proceedings of the 1st Asia-Pacific Optical Fiber Sensors Conference (IEEE, 2008), pp. 1–3.
4. M. Willsch, T. Bosselmann, M. Villnow, and W. Ecke, "Fiber optical sensor trends in the energy field," Proc. SPIE **8421**, 84210R (2012).
5. T. Bosselmann and M. Willsch, Device for measuring temperature in electromagnetic fields, US Patent 13/201,658 (Feb.16, 2012).
6. O. Frazão, L. A. Ferreira, F. M. Araújo, and J. L. Santos, "Applications of fiber optic grating technology to multi-parameter measurement," Fiber Integr. Opt. **24**(3–4), 227–244 (2005).
7. A. D. Kersey, M. A. Davis, H. J. Patrick, M. LeBlanc, K. P. Koo, C. G. Askins, M. A. Putnam, and E. J. Friebele, "Fiber grating sensors," J. Lightwave Technol. **15**(8), 1442–1463 (1997).
8. M. G. Xu, J. L. Archambault, L. Reekie, and J. P. Dakin, "Simultaneous measurement of strain and temperature using fibre grating sensors," in *10th Int. Conf. on Optical Fiber Sensors* (1994), pp. 191–194.
9. G. P. Brady, K. Kalli, D. J. Webb, D. A. Jackson, L. Reekie, and J. L. Archambault, "Simultaneous measurement of strain and temperature using the first and second-order diffraction wavelengths of Bragg gratings," in *IEEE Proceedings—Optoelectronics*, Vol. 144 (1997), p. 156.
10. L. Reekie, J. P. Dakin, J.-L. Archambault, and M. G. Xu, "Discrimination between strain and temperature effects using dual-wavelength fibre grating sensors," Electron. Lett. **30**(13), 1085–1087 (1994).
11. O. Frazão, J. P. Carvalho, L. A. Ferreira, F. M. Araújo, and J. L. Santos, "Discrimination of strain and temperature using Bragg gratings in microstructured and standard optical fibres," Meas. Sci. Technol. **16**(10), 2109–2113 (2005).
12. P. M. Cavaleiro, F. M. Araujo, L. A. Ferreira, J. L. Santos, and F. Farahi, "Simultaneous measurement of strain and temperature using Bragg gratings written in germanosilicate and boron-codoped germanosilicate fibers," IEEE Photon. Technol. Lett. **11**(12), 1635–1637 (1999).

#321223 https://doi.org/10.1364/OE.26.012092
Journal © 2018 Received 31 Jan 2018; revised 21 Mar 2018; accepted 21 Mar 2018; published 26 Apr 2018

Optics EXPRESS

13. G. Chen, L. Liu, H. Jia, J. Yu, L. Xu, and W. Wang, "Simultaneous strain and temperature measurements with fiber Bragg grating written in novel Hi-Bi optical fiber," IEEE Photon. Technol. Lett. **16**(1), 221–223 (2004).
14. J. van Roosbroeck, S. K. Ibrahim, E. Lindner, K. Schuster, and J. Vlekken, "Stretching the limits for the decoupling of strain and temperature with FBG based sensors," Proc. SPIE **9634**, 96343S (2015).
15. S. W. James, M. L. Dockney, and R. P. Tatam, "Simultaneous independent temperature and strain measurement using in-fibre Bragg grating sensors," Electron. Lett. **32**(12), 1133 (1996).
16. B. Hopf, A. W. Koch, and J. Roths, "Iterative matrix inversion technique for simultaneous strain and temperature sensing in an extended temperature range," Proc. SPIE **9916**, 99160O (2016).
17. R. R. J. Maier, W. N. MacPherson, J. S. Barton, J. D. C. Jones, S. McCulloch, and G. Burnell, "Temperature dependence of the stress response of fibre Bragg gratings," Meas. Sci. Technol. **15**(8), 1601–1606 (2004).
18. S. Spinner, "Elastic Moduli of Glasses at Elevated Temperatures by a Dynamic Method," J. Am. Ceram. Soc. **39**(3), 113–118 (1956).
19. M. Elices, and P. K. Gupta, "Strength of glass fibers," in *EURESCO Conference on High Performance Fibers: Euroconference on Fiber Fracture*, M. Elices, ed. (Elsevier, 2002), pp. 127–153.

1. Introduction

Fiber Bragg gratings (FBG) are widely used as sensors in many technical applications [1] to measure strain or temperature at various measurement points. FBG sensor arrays, with multiple FBGs in a single fiber, are especially suited for accurately monitoring temperature distributions in industrial facilities. In harsh environments and at high electromagnetic fields, such fiber optical sensors are often even the only option. Therefore, their application is of great interest for the energy-generating industry, ranging from temperature monitoring of drill holes in oil-wells [2], to temperature control of hot water pipelines in petrochemical factories [3], to monitoring engine conditions of high power generators or gas turbines [4]. As FBGs are sensitive to strain and temperature, any strain or force on the sensing fibers must be avoided during temperature measurements, which is typically achieved by mounting the sensing fiber in capillaries with a loose tube design [5]. Still, the usage of the large fiber lengths required in these applications is challenging. Friction forces between the capillary and the sensing fiber accumulate with length, adding strains to the fiber and restricting the length of sensor cables for multipoint FBG temperature measurements to a few meters. Avoiding these friction-induced forces throughout the entire fiber length represents a difficult requirement for design and installation of FBG-based multipoint temperature sensor cables. Friction significantly increases in a curved design, which limits the installation of sensor cables to an almost straight line and dramatically reduces the flexibility in the sensor setup and the routing to the demanded measurement points. If the FBG-based measurement points were nonetheless inadvertently affected by friction-induced strain, for example due to an invalid installation, the sensing system would report biased temperature readings, which could not be detected as false by the sensor system itself. Therefore, the reliability of FBG-based multipoint temperature data relies on the proper installation of the sensor cables. With the extended lengths of the sensor cables, temperature calibration can usually not be performed in the same spatial configuration, as it will be installed later in the particular application, which makes it impossible to compensate friction-induced bias by calibration.

A common solution to overcome these problems is the simultaneous detection of force and temperature by combining signals of two sensors with different sensitivities [6] multiplexed in a single fiber (sensor tandem). Assuming linear dependencies, the sensor's responses can then be described by a sensitivity matrix [6–8]. Temperature and force are derived by employing the inverted sensitivity matrix. Several approaches have been proposed during the last decade, ranging from FBGs with different Bragg wavelengths [9,10] to combining different types of fibers like photonic crystal fibers [11] or specially doped fibers [12]. Using the signals of the slow and fast axis of an FBG in a polarization maintaining fiber has been investigated as well [13,14]. Nevertheless, any large-scale use of these discrimination techniques is still pending in industrial applications, because they usually do not meet the required measurement accuracy of 1°C in the applied temperature range. Nonlinearities in the sensor characteristics generate systematic deviations when using these sensors within a large temperature range, since the linear matrix approach allows neither the

Optics EXPRESS

integration of higher order terms in the temperature response nor temperature dependent force sensitivities.

James et. al. proposed the usage of FBGs fabricated in either side of a splice joint of fibers with different cladding diameters (e.g. 80 µm and 125 µm) to simultaneously measure strain and temperature [15]. In their work, the sensing fiber was fixed to the specimen at two points left and right from the FBGs to enable full strain transfer to the fiber. In this set-up, the FBGs' temperature sensitivities would be nearly the same in both fiber types while the force sensitivity of an FBG in an 80 µm cladding fiber is about two times higher than that in a 125 µm cladding fiber. This leads to a high resolution in the discrimination of temperature and strain when using this technique. The nonlinear temperature response, however, is supposed to cause systematic deviations of several degrees when using this sensor-setup and a linear sensitivity matrix within a temperature range between –20°C and 150°C [16].

With this work, we introduce an iterative matrix algorithm that improves the measurement precision in such a sensor configuration to a large extend. For the first time to our knowledge, nonlinearities of the sensor's temperature characteristics as well as the temperature dependence of the force sensitivities were included in the algorithm for decoupling temperature and axial force.

This principle for multi-parameter measurements was applied to force-compensated temperature measurements with a sensor cable consisting of an FBG sensor tandem installed in a 7 m-long coiled PEEK capillary. Temperature measurements were performed in an extended temperature range from –35°C to 125°C. Although friction-induced forces up to 1.6 N developed in the sensor fiber, the determined temperatures deviated less than 0.5°C from their reference values. Therefore, a new and accurate method is now available that enables reliable quasi-distributed FBG-based temperature measurements within uncertainties less than one degree Celsius, even when using long cable lengths of several meters.

2. Theory

One tandem FBG element consists of a short piece of a single mode fiber with 80 µm diameter spliced between a fiber with 125 µm in diameter as depicted in Fig. 1. FBGs are located directly at the left and the right side of the splice joint in the 80 µm and the 125 µm diameter fiber. Any axial force acting on the fiber is assumed to be the same for both FBGs, as is the temperature.

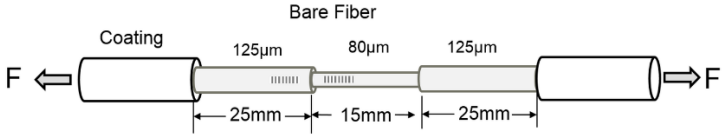

Fig. 1. Schematic of the sensor element: A small piece of an 80 µm diameter fiber (ca. 15 mm) is positioned between a 125 µm cladding fiber. FBGs are located at each side of the splice joint. Temperature and force are supposed to be the same in both FBGs. Due to the different cladding diameters, the force sensitivity is about 2.4 times higher for the 80 µm fiber than for the 125 µm diameter fiber, while temperature sensitivities are nearly the same for both fiber types. The signals of both FBGs can be used to determine temperature and force acting on the fiber.

In general, (1) gives the change in Bragg wavelength $\Delta\lambda_B(\Delta T)$ of an FBG due to temperature changes $\Delta T = T - T_0$, (1.2) the change in Bragg wavelength $\Delta\lambda_B(F)$ due to an axial force F,

$$\Delta\lambda_B(\Delta T) = \lambda_{B,0}(\alpha+\xi)\cdot\Delta T = K_T\cdot\Delta T, \tag{1}$$

$$\Delta\lambda_B(F) = \lambda_{B,0}\frac{1-p_{eff}}{A\cdot E}\cdot F = K_F\cdot F. \tag{2}$$

Optics EXPRESS

Here, α is the fiber's coefficient of thermal expansion, ξ the thermo-optical coefficient, and $\lambda_{B,0}$ the Bragg wavelength at zero strain at reference temperature T_0 (e.g. room temperature). The factor $\lambda_{B,0}(\alpha+\xi)=K_T$ may be summarized in the temperature sensitivity constant K_T as in (1). In (1), p_{eff} is the strain optical coefficient, E the fiber's Young's modulus and A the fiber's cross-section area. The product of these influences is summarized in a strain sensitivity constant K_F. Except for the cross-section area A, all influencing factors are material characteristics of glass, and are supposed to be nearly similar in both fiber types. The cross-section area differs by a factor 2.44, leading to high differences in the force sensitivities of the two fibers.

Assuming linear dependencies of the Bragg wavelengths to environmental influences (in this case force F and temperature change $\Delta T = T - T_0$), the responses of the two FBGs can be written with a sensitivity matrix of the form [15]

$$\begin{pmatrix} \Delta\lambda_{B,80\mu m} \\ \Delta\lambda_{B,125\mu m} \end{pmatrix} = \begin{pmatrix} K_{T,80\mu m} & K_{F,80\mu m} \\ K_{T,125\mu m} & K_{F,125\mu m} \end{pmatrix} \cdot \begin{pmatrix} \Delta T \\ F \end{pmatrix}, \tag{3}$$

The indices "80µm" and "125µm" mark the values derived from the FBG in the 80 µm and 125 µm fiber, respectively. $\Delta\lambda_{B,80\mu m}$ and $\Delta\lambda_{B,125\mu m}$ are the changes in Bragg wavelengths due to changes in temperature ΔT and force F. Matrix inversion provides the temperature and force values derived from the measured wavelengths of the two FBGs, according to

$$\begin{pmatrix} \Delta T \\ F \end{pmatrix} = \frac{1}{D} \begin{pmatrix} K_{F,125\mu m} & -K_{F,80\mu m} \\ -K_{T,125\mu m} & K_{T,80\mu m} \end{pmatrix} \cdot \begin{pmatrix} \Delta\lambda_{B,80\mu m} \\ \Delta\lambda_{B,125\mu m} \end{pmatrix}, \tag{4}$$

with $D = K_{T,125\mu m} \cdot K_{F,80\mu m} - K_{T,80\mu m} \cdot K_{F,125\mu m}$.

As a first approximation, the linear dependency holds for the FBG's force and temperature characteristics. Nevertheless, if the linear approach (4) is applied, nonlinearities in the temperature dependency, lead to significant systematic errors, which are in the order of several degree Celsius for extended temperature ranges from e.g. –20°C to 150°C.

At a given constant temperature, a linear function is sufficient to describe the dependence of the Bragg wavelength on axial force. However, it has been shown that an FBG's response to stress, and therefore its response to force as well, depends on temperature [17]. This cross-sensitivity is also not taken into account in the linear approach described by (4), representing a further source of systematic error.

An iterative matrix approach for force and temperature discrimination eliminates these systematic uncertainties. Starting with the matrix values for reference temperature (j = 0, $\Delta T = 0\,°C$) temperature and force values are calculated iteratively according to

$$\begin{pmatrix} \Delta T^j \\ F^j \end{pmatrix} = \frac{1}{D(\Delta T^{j-1})} \begin{pmatrix} K_{F,125\mu m}(\Delta T^{j-1}) & -K_{F,80\mu m}(\Delta T^{j-1}) \\ -K_{T,125\mu m}(\Delta T^{j-1}) & K_{T,80\mu m}(\Delta T^{j-1}) \end{pmatrix} \begin{pmatrix} \Delta\lambda_{B,80\mu m} \\ \Delta\lambda_{B,125\mu m} \end{pmatrix}, \tag{5}$$

with $D(\Delta T) = K_{T,125\mu m}(\Delta T) \cdot K_{F,80\mu m}(\Delta T) - K_{T,80\mu m}(\Delta T) \cdot K_{F,125\mu m}(\Delta T)$.

For each step j, the temperature value from the preceding iteration step (j-1) is used to determine the new matrix values.

Previous investigations have shown that third order polynomial functions are suitable to describe the temperature response of FBG sensor elements accurately [17–19].

The change in Bragg wavelength according to temperature changes can be written in the form

Optics EXPRESS

$$\Delta\lambda_{B,k}(\Delta T) = \left(a_{T,k} + b_{T,k}\Delta T + c_{T,k}\Delta T^2\right)\Delta T \equiv K_{T,k}(\Delta T)\,\Delta T \tag{6}$$

The term $\left(a_{T,k} + b_{T,k}\Delta T + c_{T,k}\Delta T^2\right)$ can be taken as a definition for the temperature dependent matrix elements $K_{T,k}(\Delta T)$, where k indicates the corresponding fiber's diameter, i.e. k = 80 µm or k = 125 µm.

In this study, the force sensitivity of the Bragg grating sensor elements is assumed to decrease linearly with temperature. The changes in Bragg wavelength as a function of the acting force is given by

$$\Delta\lambda_{B,k}(F) = a_{F,k}\left(1 + b_{F,k}\Delta T\right)F \equiv K_{F,k}(\Delta T)\,F \tag{7}$$

where $a_{F,k} \equiv K_{F,k}(\Delta T = 0°\text{C})$ is the force sensitivity at reference temperature, and $b_{F,k} = \left(K_{F,k}(\Delta T) - a_{F,k}\right)/\left(a_{F,k}\Delta T\right)$ the relative change of the force sensitivity with temperature. $K_{F,k}(\Delta T)$ are the temperature-dependent force sensitivity matrix elements for the corresponding types of fibers (with k = 80 µm or k = 125 µm, respectively).

The iteration steps are repeated until the values for temperature and force have converged (typically three times). Since nearly all kind of nonlinearities may be implemented in the evaluation process, this method provides a powerful tool for accurate multi-parameter measurements, even in a large temperature range.

3. Experimental

3.1. Sensor setup and calibration

A 15 mm long piece of a 1310-HP-80 fiber (Nufern, East Granby, CT, USA) with 80 µm cladding diameter was spliced between a SMF28 standard telecom fiber with an LFS4100 filament splicing unit (Vytran UK Thorlabs Ltd, Exeter, Great Britain). The obtained geometry is depicted in Fig. 1.

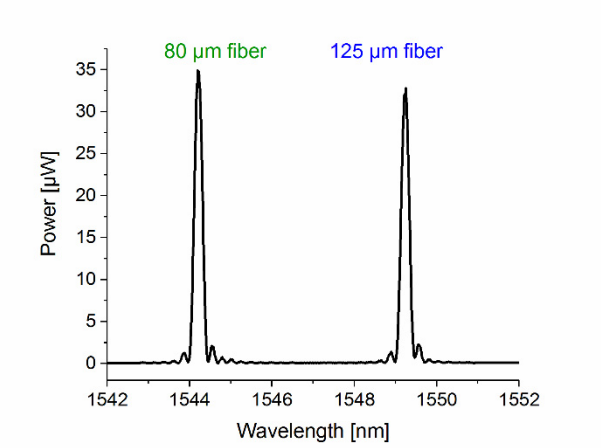

Fig. 2. Spectra of the FBGs in the 80 µm and 125 µm fiber at 24°C: The Bragg wavelength of 1544 nm corresponds to the grating in the fiber with 80 µm cladding diameter, the Bragg wavelength of 1549 nm to the grating in the fiber with 125 µm.

Both fibers match in mode field diameter and in numerical aperture resulting in low splicing losses. The coating was stripped off the fibers near the splicing joints 25 mm in length in the 125 µm fiber and over the whole 15 mm of the 80 µm fiber analogous to Fig. 1. Uniform gratings with 4 mm length were inscribed on either side of one of the splicing joints

Optics EXPRESS

using our in-house inscription facility, which is based on a 248 nm KrF-Exciplex laser combined with a phase mask technique. The periods of the gratings, determined from the phase mask period, were about 530 nm in the 80 µm fiber and 535 nm in the 125 µm fiber. The corresponding FBG spectra measured at 24°C are shown in Fig. 2.

For temperature calibration, the sensing element has been exposed to a temperature cycle in a climatic chamber (VCL 4010: Vötsch GmbH, Balingen, Germany). Figure 3 (a) shows the experimental setup. The fiber has been vertically suspended in the chamber with no contact to the surrounding surfaces to avoid friction-induced mechanical forces in the fiber during temperature changes. A calibrated Pt100 was placed next to the FBGs for reference temperature measurements. The temperature was increased stepwise from –40°C to 175°C in steps of 20°C and then decreased to –40°C, again in steps of 20°C. Each temperature value was held for one hour. At the end of each temperature step the Bragg wavelengths were measured 20 times with a SM125 tunable laser interrogator (Micron Optics, Atlanta, USA) with a wavelength uncertainty of 2 pm.

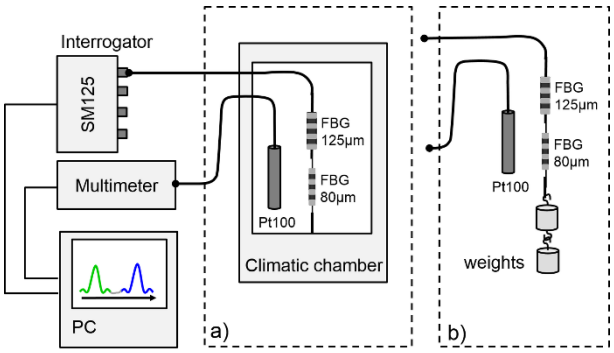

Fig. 3. Measurement setup using a tunable laser interrogator (SM125, Micron Optics) for Bragg wavelengths determination: a) Temperature calibration was carried out on vertically suspended sensor elements in a climatic chamber. b) Weights were applied to the fiber for force calibration. A calibrated Pt100 was used for temperature reference.

A temperature of T_0 = 24°C was chosen as reference temperature. Both, a linear function $\lambda_{B,k}(T) = \lambda_{0,k} + a_{T,k}(T - T_0)$ and a polynomial function $\lambda_{B,k}(T) = \lambda_{0,k} + a_{T,k}(T - T_0) + b_{T,k}(T - T_0)^2 + c_{T,k}(T - T_0)^3$ were fitted to the measured Bragg wavelengths for the FBGs in both types of fibers (with k = 125 µm and k = 80 µm diameters). The fit values are summarized in Tab. 1. For the linear matrix approach (4), $K_{T,k} = a_{T,k} = const.$ was used, where $a_{T,k}$ are the parameters derived from the linear fit. For the iterative matrix approach (5), the temperature dependent matrix elements are given as $K_{T,k}(\Delta T) = a_{T,k} + b_{T,k}\,\Delta T + c_{T,k}\,\Delta T^2$. Figure 4 shows the changes of the Bragg wavelengths $\Delta\lambda_{B,k} = \lambda_{B,k}(T) - \lambda_{0,k}$ with temperature for both FBGs, with $\lambda_{0,80\mu} = 1544.229$ nm and $\lambda_{0,125\mu} = 1549.248$ nm taken from the polynomial fit. The (blue) triangles mark the values for the FBG in the 125 µm fiber, the (green) dots for the FBG in the 80 µm fiber. The third order polynomial fit functions (green curve for the 80 µm fiber, blue curve for the 125 µm fiber) and the linear fit functions (red line for the 80 µm fiber, black line for the 125 µm fiber) are also depicted in Fig. 4. Both sensors show nearly the same sensitivities to temperature, with no sign of hysteresis, but with a significant nonlinear behavior. When fitted linearly, systematic wavelengths deviations between the measured wavelengths and the linear fit function of approx. 70 pm at –40°C and at 170°C and –40 pm at 60°C were observed for both FBGs. With a 3rd order polynomial fit, the residuals (difference of measured values to the fit)

Optics EXPRESS

scatter around zero with a standard deviation of 2.7 pm and 2.4 pm for the 80 µm and 125 µm cladding diameter fiber, respectively.

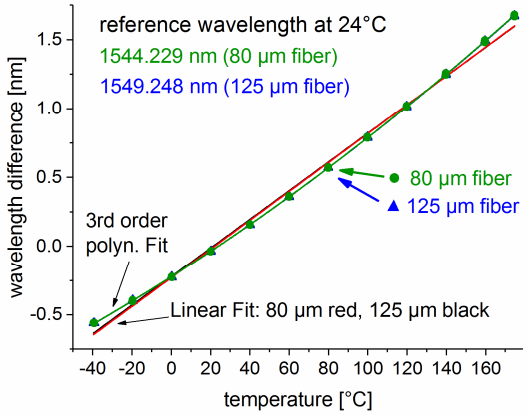

Fig. 4. Temperature sensitivity: Change of Bragg wavelength $\Delta\lambda_{B,k} = \lambda_{B,k} - \lambda_{0,k}$ as a function of temperature and the corresponding linear fits and the 3rd order polynomial fits The values of the FBG in the 80 µm fiber are depicted in green, the values of the 125 µm fiber in blue.

Force calibration was performed with the same sensor element at room temperature (approx. 24°C). The experimental setup is depicted in Fig. 3 (b). The fiber was stretched during two cycles of increasing weights up to 1.6 N in steps of approx. 0.25 N. The weights were then removed in steps to zero. The Bragg wavelength was measured 20 times at every step. Figure 5 shows the changes in Bragg wavelength $\Delta\lambda_{B,80\mu m} = \lambda_{B,80\mu m} - \lambda_{0,80\mu m}$ and $\Delta\lambda_{B,80\mu m} = \lambda_{B,125\mu m} - \lambda_{0,125\mu m}$ due to applied forces, where $\lambda_{0,80\mu m}$ and $\lambda_{0,125\mu m}$ are the Bragg wavelengths of the 80 µm and 125 µm without external stress at room temperature, respectively. The (green) dots mark the measured values for the 80 µm fiber, the blue triangles the values of the 125 µm fiber. Linear functions were fitted to both curves.

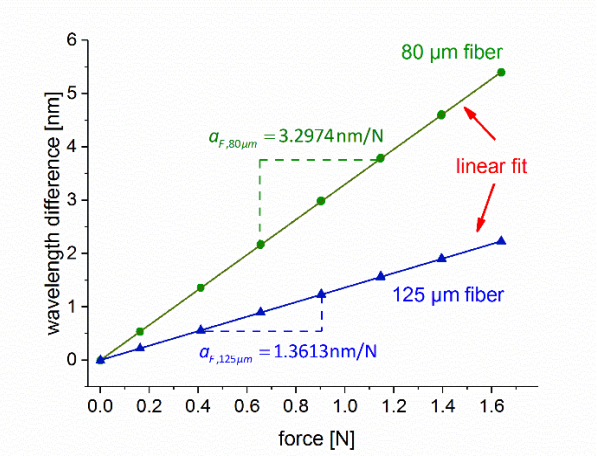

Fig. 5. Force sensitivities $a_{F,k}$ at room temperature: Change of Bragg wavelength $\Delta\lambda_{B,k} = \lambda_{B,k} - \lambda_{0,k}$ as a function of the applied force and the corresponding fits of linear functions. The values of the FBG in the 80 µm fiber are depicted with green dots, the values of the 125 µm fiber with blue triangles.

Optics EXPRESS

The slopes are equivalent to the force sensitivities at reference temperature, $a_{F,k}$. The fit values are given in Table 1 (Force sensitivity). The force sensitivity is 2.43 times as high for the FBG in the 80 µm fiber compared to the FBG in the 125 µm fiber, which corresponds to the theoretical prediction given by the cross-section area-ratio of $(125/80)^2 = 2.44$. The residuals scatter statistically around zero with a standard deviation of 2.9 pm and 2.5 pm for the 80 µm and 125 µm cladding fiber, respectively, without any hysteresis.

The temperature dependencies of the force sensitivities were estimated separately with two single FBGs in an 80 µm and a 125 µm fiber, respectively. At different controlled temperatures, weights with increasing values up to 0.86 N (5 steps) were applied to vertically suspended fibers. The weights were then removed stepwise down to zero, proving the absence of hysteresis behavior. As depicted in Figs. 6 (a) and 6 (b), two different setups were used to stabilize the FBGs at constant temperatures. At 4°C, 20°C, 40°C and 50°C, the fibers were suspended in a 1 mm hole in a copper block, which was temperature controlled by a Peltier element (TED 200C: Thorlabs GmbH, Dachau, Germany). A ROS 20/250/12 tube furnace (ThermConcept GmbH, Bremen, Germany) was employed to stabilize at 97°C, which was the lowest operation temperature of the furnace.

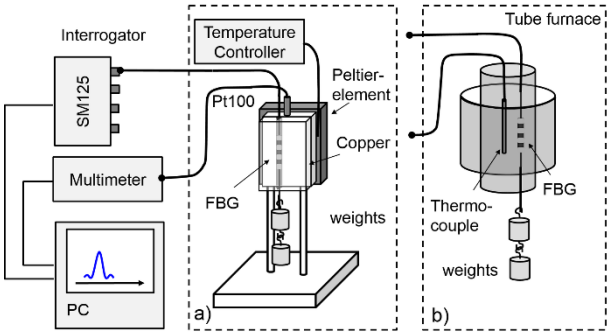

Fig. 6. Measurement setup for temperature dependency of the force sensitivity. Temperature stabilization was obtained a) with a Peltier element (TED 200C: Thorlabs GmbH) in the temperature range between 4°C and 50°C, b) with a tube furnace (ROS 20/250/12: ThermConcept GmbH) at 97°C.

The relative changes of the force sensitivities as a function of temperature, $b_{F,k}$, is depicted in Fig. 7. The reference temperature was 24°C. Green circles mark the values the 80 µm fiber measured in the tube furnace, green dots the values of the FBG temperature stabilized with the Peltier element. The values of the 125 µm fiber are marked with blue triangles.

With increasing temperature, the FBG's force sensitivities decreased by 1.52% and 0.95% every 100°C in the 80 µm and 125 µm fiber, respectively. Fused silica is known for its increase in the Young's modulus with increasing temperatures of about 1% every 100°C [18], which is assumed here to be the main reason for the fiber's reduction in force sensitivity [17]. This correlates well with the temperature dependence of the force sensitivity in the 125 µm fiber of 0.95% every 100°C. Additionally, a strong skin effect is known for fused silica [17], where the strength of a fiber (i.e. braking stress) scales nonlinearly with decreasing fiber diameters [19]. This is accompanied by commensurate higher Young's moduli in fibers with smaller diameters [17,19]. which may explain the observed higher temperature dependency in the 80 µm fiber of 1.52% every 100°C. The relative change of the force sensitivity with temperature, $b_{F,k}$,is supposed to be a characteristic of each fiber type.

Optics EXPRESS

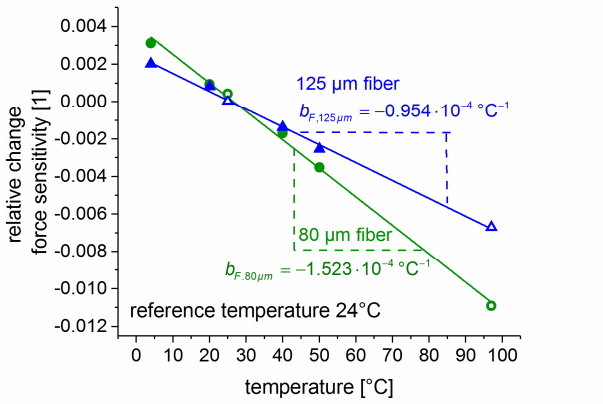

Fig. 7. Relative change in force sensitivity $b_{F,k}$ as a function of temperature: The values of the FBG in the 80 µm fiber are depicted with green dots, the values of the 125 µm fiber with blue triangles.

The values were applied as temperature-dependent sensitivity elements to the force calibration of the tandem-sensor element, as summarized in Table 1.

Table 1. Force and temperature sensitivities

Temperature sensitivity	**Fiber diameter, *k***	**λ_0 (T = 24°C,F = 0 N) [nm]**	**a_T [nm/°C]**	**b_T [nm/°C^2]**	**c_T [nm/°C^3]**
3rd order polyn. fit	80 µm 125 µm	1544.229 1549.248	0.00904 0.00904	$1.237 \cdot 10^{-5}$ $1.230 \cdot 10^{-5}$	$-1.098 \cdot 10^{-8}$ $-1.074 \cdot 10^{-8}$
Linear fit	80 µm 125 µm	1544.258 1549.278	0.01043 0.01042		
Force sensitivity	**Fiber diameter, *k***	**λ_0 (T = 24°C,F = 0 N)**	**a_F [nm/N]**	**b_F [1/°C]**	
Cross sensitivity	80µm 125µm	1544.229 1549.248	3.2974 1.3613	$-1.523 \cdot 10^{-4}$ $-0.954 \cdot 10^{-4}$	

3.2. Friction compensation for temperature measurement with an FBG mounted in a 7m long capillary with loose-tube design

The capability of the above-described force- and temperature-discrimination was demonstrated for friction-compensated temperature measurements in a real-world scenario. For this purpose, one FBG-based temperature measurement point was realized in the middle of a seven meter long sensor fiber, which was installed in a PEEK capillary with a loose-tube design. In order to simulate a complex fiber routing to the measurement pint, the capillary was coiled on both sides of the measurement point. Due to the length and the curved shape, significant friction between the optical fiber and the capillary is expected. Any temperature changes would therefore lead to high axial forces caused by the differences in the fiber's and the capillary's coefficient of thermal expansion. Thus, this system can be regarded as a worst-case scenario for a temperature sensing point in a long, multipoint sensor fiber with complex fiber routing.

A three and a four meter long SMF28 fiber was spliced on both ends of the sensor-tandem element as depicted in Fig. 1 to extend the total length of the fiber sensor. The fiber had been exposed to 170°C for one hour to age the acrylate coating and was then placed in an 7 m long PEEK-capillary with an inner diameter of 1.2 mm. In the area of the FBGs, the capillary was mounted with tape on a straight aluminum rod of 300 mm in length. On both sides of the sensor elements, the rest of the capillary was coiled to diameters of about 300 mm. The whole

Optics EXPRESS

arrangement was placed in the climatic chamber (see Fig. 8). A calibrated Pt100 was placed next to the FBGs for reference temperature measurements.

The temperature was increased from −35°C up to 125°C in steps of 20°C. At each step, the temperature was held stable for 30 minutes. The Bragg wavelengths were determined continuously every minute using the experimental setup described in Fig. 8.

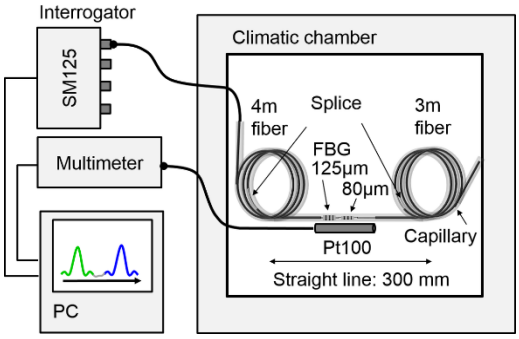

Fig. 8. Schematic of the dimensions and locations of the sensor element in the PEEK capillary and measurement setup.

The results are shown in Fig. 9. The change in Bragg wavelength of the FBG in the 80 µm fiber is depicted with (green) dots, of the FBG in the 125µm fiber with (blue) triangles as a function of time. The (red) line refers to the temperature reference (Pt100) plotted versus time. The scale markings for temperature correspond to the wavelength difference if assuming a temperature sensitivity of 10.4 pm/°C.

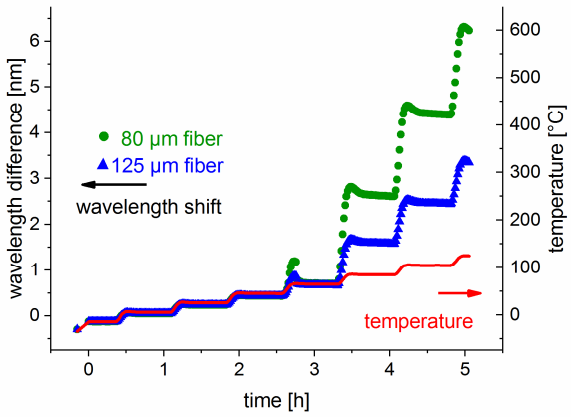

Fig. 9. Bragg wavelength shifts $\Delta\lambda_{B,k} = \lambda_{B,k} - \lambda_{0,k}$ of the tandem sensor element as a function of time. The values of the FBG in the 80 µm fiber are depicted in green, the values of the 125 µm fiber in blue and the temperature measured with a calibrated Pt100 in red. The scale markings for temperature correspond to the wavelength difference if assuming a temperature sensitivity of 10.4 pm/°C.

Up to 2.5 hours, which correspond to the temperature steps from −35°C to 45°C, the changes in Bragg wavelength fit the changes of temperature. With any further increase in temperature, the measured Bragg wavelengths of the two FBG deviate from the temperature curve, leading to an increasing gap between the temperature curve and the measured wavelengths. This means that assuming a constant temperature sensitivity of 10.4 pm/°C as the only source of the FBGs' wavelength shift would lead to strongly biased temperature readings if exceeding 65°C. A maximal deviation of 160°C and 280°C for the 80 µm and 125

Optics EXPRESS

µm fiber, respectively, was reached at 125°C. Significant axial forces acting on the fiber during heating are the main cause for this discrepancy. With increasing temperature, the expansion of the PEEK-capillary is much larger than the thermal expansion of the fiber. Friction in the capillary, especially in the coiled regions, prevented the fiber from slipping, leading to increasing forces on the FBGs at higher temperature. At the beginning of each temperature step, a peak is visible in the Bragg wavelength change, with a decrease in wavelength shortly after the set temperature was reached. This indicates a partial relaxation of the strained fibers in the capillary during the first minutes after the temperature change. The force-induced increase of Bragg wavelengths in the 80 µm fiber (green dots) was much larger compared to the increase in the 125 µm fiber (blue triangles). This is a consequence of the different diameters of the fibers. After five hours, at a temperature of 125°C and a total wavelength shift of nearly 7 nm, the 80 µm fiber ripped due to the high tensile forces, which are related to a strain of approx. 4500 µstrain in the 80 µm fiber.

4. Results and discussion

4.1. Temperature-force decoupling

Using the combination of both FBGs allows discriminating strain and temperature influences from the measured Bragg wavelengths. The blue circles in Fig. 10 show the temperature values obtained with the standard (linear) matrix approach of (4) using constant matrix elements ($K_{F,k} = const.$ and $K_{T,k} = const.$) plotted against reference temperature. The evaluated temperatures deviate systematically from the identity line depicted in red. The temperature values obtained after three iteration cycles with the iterative matrix approach (5) using temperature dependent matrix elements for both, the temperature and the stain sensitivities ($K_{F,k}(\Delta T)$ and $K_{T,k}(\Delta T)$), are plotted with dark blue dots in Fig. 10. By implementing the nonlinearities of the temperature characteristics and the cross-sensitivity of strain and temperature in the evaluation process, the temperatures calculated from the FBG sensor element accurately match the values of the Pt100 temperature reference in the entire measurement range between −35°C and 125°C. This demonstrates the capability of the iterative matrix method to correct deviations due to friction-induced strains on the fiber and nonlinearities in the sensor's temperature characteristics.

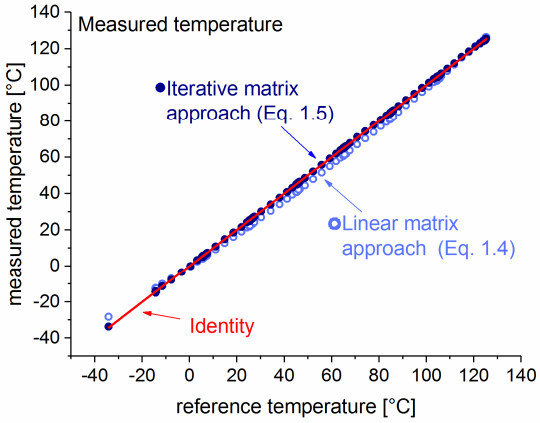

Fig. 10. Nonlinear iterative matrix approach: The determined temperatures of the linear matrix method with constant matrix elements (blue circles) are compared to the results of the iterative matrix method with temperature dependent force and temperature sensitivities after three iteration cycles (blue dots), plotted against the reference temperatures of the Pt100 (red line: identity). The temperatures evaluated with the iterative matrix method match the values of the Pt100 reference in the whole temperature range.

Optics EXPRESS

The corresponding force versus reference temperature is depicted in Fig. 11 for the linear matrix approach (blue circles) and the iterative approach with temperature dependent matrix elements (dark blue dots). Above 60°C, the force increased nearly linearly with temperature reaching maximum values of 1.6 N at 125°C.

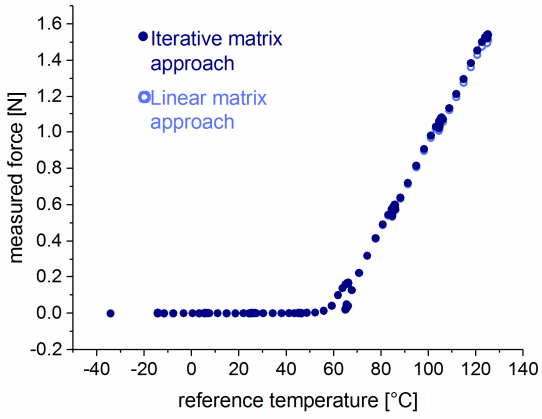

Fig. 11. Nonlinear iterative matrix approach: The determined force values of the linear matrix method with constant matrix elements (blue circles) and the values obtained with the iterative matrix method using temperature dependent force and temperature sensitivities after three iteration cycles (blue dots) are plotted against the reference temperatures of the Pt 100. There is no evidence for friction-induced forces for temperatures below 55°C. Higher temperatures led to increasing forces with 1.6 N at 125°C.

4.2. Enhanced accuracy with iterative matrix approach

For a large-scale application in an industrial environment, it is essential to ensure low uncertainties of less than 1°C in a large temperature range. In order to evaluate the relative influence of the non-linear temperature characteristics and the temperature dependence of the force sensitivity, the data was evaluated with three different methods: a) with the standard linear matrix approach of (4), b) with nonlinear temperature characteristics $K_{T,k}(\Delta T)$ and constant force sensitivity $K_{F,k}$ in (5) and, c) with temperature dependent matrix elements for both, $K_{T,k}(\Delta T)$ and $K_{F,k}(\Delta T)$ in (5). Here, for each temperature step, the last 20 data points at constant temperatures were averaged. For the three evaluation methods, the deviations of the calculated FBG-based temperature values to the reference temperatures are shown in Fig. 12 for the three evaluation methods.

The values derived from the linear matrix approach (4) with constant matrix elements as given in Table 1 (temperature sensitivity: linear fit and force sensitivity a_F) are depicted with black cycles. Systematic deviations of several degree Celsius were detected. The largest discrepancy to the reference was a positive deviation of 6°C at −35°C, which is the lower border of the temperature calibration range, and a negative deviation of approx. 4°C between 45°C to 85°C in the middle of the calibration range. The linear approximations to the nonlinear temperature characteristics of the FBGs in both types of fibers contribute dominantly to these deviations. Since temperature calibrations were performed in a larger temperature range from –40°C to 170°C (see Fig. 4), while the highest temperature in multi-parameter sensing was approx. 130°C, the deviations are highly non-symmetric in the temperature range depicted in Fig. 12.

Optics EXPRESS

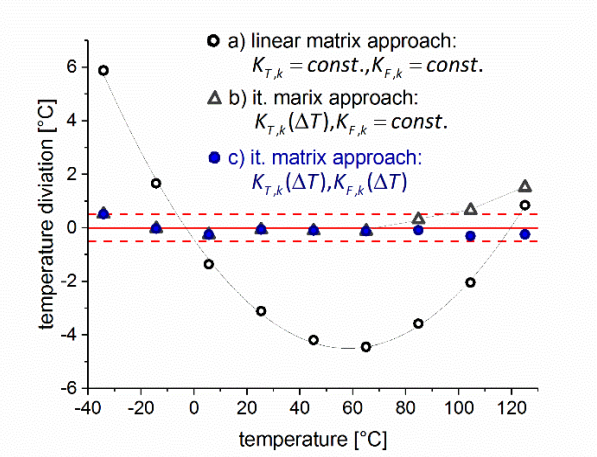

Fig. 12. Deviations of the FBG-based temperature values from reference temperature evaluated with different approaches: Circles: Linear matrix approach with constant matrix elements. Triangles: Iterative matrix solution with nonlinear temperature characteristics and constant force sensitivity. Dots: iterative matrix solution with nonlinear temperature characteristics and temperature-dependent force sensitivities.

The systematic deviations due to the nonlinear temperature characteristics could significantly be reduced by using the temperature dependent matrix elements $K_{T,k}(\Delta T)$, while still assuming constant force sensitivities $K_{F,k} = a_{F,k}$ (method b) for both fibers. The data evaluated with this configuration are depicted with triangles in black color in Fig. 12. In the lower temperature range up to 85°C the deviations now stay within a range of 0.5°C around the reference temperature (confined by the red dashed lines). For high temperatures (85°C to 125°C) the deviations increase significantly with temperature to values of about 2°C. As it is evident from Fig. 11, increasing axial forces acted on the fiber in this temperature range, indicating that this discrepancy is caused by a temperature dependence of the FBG's force sensitivities. The blue dots mark the difference between the determined and the reference temperatures if the temperature dependence of both, $K_{T,k}(\Delta T)$ and $K_{F,k}(\Delta T)$ was considered. Hence, all temperature values stayed within 0.5°C around the reference temperature values (mean value: –0.2°C; standard deviation: 0.2°C), making this method a very powerful tool for accurate temperature measurements in the presence of friction if using long fiber lengths and complicated fiber routing.

5. Conclusion

Multi-parameter measurement techniques, especially force and temperature discrimination, are highly in demand in FBG-based sensing applications. Commonly, the response of two FBGs with different sensitivities, described by a linear sensitivity matrix with constant matrix elements, is used to calculate temperature and force. Here, we applied a novel iterative matrix algorithm that allows including nonlinearities of the sensor's temperature characteristics and the temperature dependence of the sensor's force sensitivities in the evaluation process. This technique was applied to temperature and force measurements in a temperature range between –35°C to 125°C with a sensor configuration based on FBGs in fibers with 80 µm and 125 µm cladding diameters in a 7m-long PEEK-capillary with coiled ends. Using this sensor configuration with a linear matrix approach and constant matrix elements still led to systematic deviations of up to 6°C mainly caused by nonlinearities in the sensor's temperature characteristics. Including temperature-dependent matrix elements in the evaluation algorithm was a fundamental ground to improve the precision in the friction-

Optics EXPRESS

compensated temperature measurements. Taking nonlinearities in the temperature sensitivities into account, while neglecting any temperature dependence of the force sensitivities, enabled temperature measurements with an uncertainty of 0.5°C for temperatures below 85°C. At higher temperatures and at high friction-induced forces up to 1.6 N the deviations from the reference temperature increased to nearly 2°C at 125°C. Additionally, adding the temperature dependence of the force sensitivity enabled highly precise friction-compensated temperature measurements in the whole temperature range from −35°C up to 125°C, in which the determined temperatures deviated less than 0.5°C from their reference values. Therefore, a new and accurate method is now available that enables reliable quasi-distributed FBG-based temperature measurements within uncertainties of less than one degree Celsius, even when using long cable lengths of several meters.

Funding

Federal Ministry of Education and Research (BMBF) of Germany: 03FH055PX3; Bavarian Research Foundation (BFS): AZ-1146-14; German Research Foundation (DFG): NI1911/1-1.